

A&A manuscript no.  
(will be inserted by hand later)

Your thesaurus codes are:  
(11.01.2; 11.10.1; 11.17.4:S5 0836+710; 13.18.1)

ASTRONOMY  
AND  
ASTROPHYSICS

# VSOP imaging of S5 0836+710: a close-up on plasma instabilities in the jet

A.P. Lobanov<sup>1</sup>, T.P. Krichbaum<sup>1</sup>, A. Witzel<sup>1</sup>, A. Kraus<sup>1</sup>, J.A. Zensus<sup>1</sup>, S. Britzen<sup>1,2</sup>, K. Otterbein<sup>1,3</sup>, C.A. Hummel<sup>4</sup>, and K. Johnston<sup>4</sup>

<sup>1</sup> Max-Planck-Institut für Radioastronomie, Auf dem Hügel 69, D-53121 Bonn, Germany

<sup>2</sup> The Netherlands Foundation for Research in Astronomy, P.O.Box 2, 7990 AA Dwingeloo, The Netherlands

<sup>3</sup> Landessternwarte Heidelberg, Königstuhl, D-69117 Heidelberg, Germany

<sup>4</sup> United States Naval Observatory, Washington, D.C., USA

Received 19 August 1998 / Accepted 21 September 1998

**Abstract.** The luminous high-redshift ( $z = 2.17$ ) quasar S5 0836+710 has been observed at 5 GHz with the VSOP. We compare the properties of three images obtained from the observation: a low-resolution ground array image (dynamic range 4600:1), a full-resolution VSOP image (900:1), and an image made with only the space baselines (200:1). The space baselines alone are sufficient for a reliable recovery of the source structure, within the limits of the achieved spatial sampling of the visibility data. The curved jet ridge line observed in the images can be described by Kelvin-Helmholtz instabilities developing in a relativistic outflow with the Mach number of about 6. This description holds on the scales of  $\lesssim 700 h^{-1} \text{pc}$ , and is shown to be consistent with variable apparent speeds observed in the jet.

**Key words:** galaxies: active – galaxies: jets – quasars: individual: 0836+710 – radio continuum: galaxies

## 1. Introduction

The VSOP (VLBI<sup>1</sup> Space Observatory Program) is a Space VLBI (SVLBI) mission utilizing the worldwide array of radio telescopes and an orbiting 8-meter antenna deployed on the Japanese satellite HALCA<sup>2</sup> (Hirabayashi 1996). The satellite has an elliptical orbit, with the apogee at 21 000 km, perigee at 560 km, and orbiting period of about 6 hours. In each observation, the data stream from the satellite is recorded by a network of 5 STS (Satellite Tracking Station), and subsequently correlated with the data from participating ground telescopes. Regular VSOP observations started in September 1997 at 1.6 and 5 GHz. A 5 GHz VSOP observation

of 0836+710 (4C71.07,  $z=2.17$ ) was made on October 7, 1997. This radio source is an ultraluminous quasar with well established, correlated (Otterbein et al. 1998) broadband variability in gamma-ray (Fichtel et al. 1994), X-ray (Brunner et al. 1994), optical (von Linde et al. 1993), mm- and cm- radio regimes (Marscher & Bloom 1994). The source has a well collimated VLBI-scale jet (Hummel et al. 1992) extending out to  $\sim 180$  milliarcseconds (mas). The jet is substantially curved, with lateral displacements of its ridge line and oscillations of its transverse width (possibly correlated with the observed jet speeds, Krichbaum et al. 1990). The observed speeds change remarkably along the jet: near the core, apparent speeds  $\beta_{\text{app}} \approx 10 h^{-1} c$  are measured (with  $q_0 = 0.5$  and  $H_0 = 100 h \text{ km s}^{-1} \text{ Mpc}^{-1}$ ); at 3 mas core separation, the speed decreases down to  $\beta_{\text{app}} \sim 2-3 h^{-1} c$ , and then becomes larger once again, further out (Krichbaum et al. 1990, Otterbein 1996). This kinematic behavior may be caused by MHD instabilities developing in the jet plasma (Hummel et al. 1992).

We present here a 0.2-mas ( $0.8 h^{-1} \text{pc}$ ) resolution VSOP image of 0836+710, and discuss the morphology and properties of the compact jet in this quasar.

## 2. VSOP observation and data reduction

0836+710 was observed with the VSOP at 5 GHz for 11.5 hours, with the VLBA<sup>3</sup> array (see Zensus, Diamond, & Napier 1995, and references therein) providing ground support for the observation. The data were recorded in the VLBA format, using total observing bandwidth of 32 MHz divided in two intermediate frequency (IF) bands, each having 256 spectral channels. The STS in Usuda (Japan), Tidbinbilla (Australia), and Robledo (Spain) were used for the satellite data acquisition. The data were correlated at the VLBA correlator in Socorro, with output pre-

Send offprint requests to: A.P. Lobanov

<sup>1</sup> Very Long Baseline Interferometry

<sup>2</sup> Highly Advanced Laboratory for Communication and Astronomy

<sup>3</sup> Very Long Baseline Array of the National Radio Astronomy Observatory, USA

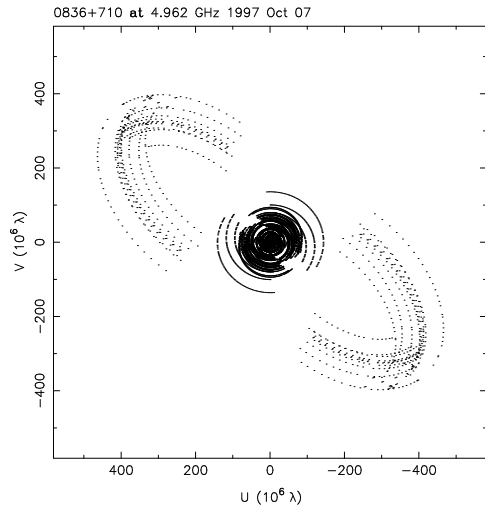


**Fig. 1.** The  $uv$ -coverage the VSOP observation of 0836+710. The inner circles correspond to the baselines between ground radio telescopes; the space baselines are grouped into larger ellipses extending at a P.A.  $\approx 45^\circ$ .

averaging time of 1.966 and 0.524 seconds for the ground and space baselines respectively. Fringe visibilities were detected in the HALCA data recorded at Tidbinbilla and Robledo. The resulting sampling function ( $uv$ -coverage) of the final correlated dataset is shown in Figure 1, indicating an improvement of resolution by a factor of  $\sim 3$  compared to ground VLBI observations at the same frequency.

### 2.1. Fringe fitting

Post-processing of the correlated data has been done in AIPS<sup>4</sup> and DIFMAP (Shepherd et al. 1994). We applied amplitude calibration, using the antenna gain factors and system temperature measurements. After inspecting the IF bandpasses, the last 46 channels were flagged in each IF, owing to significant (50-80%) amplitude reduction. This has reduced the total observing bandwidth to 26.2 MHz. We applied the phase-cal information available for the VLBA antennas, and then corrected the residual delays and rates, using the single-band (SB) and multi-band (MB) delay fringe fitting. We used solution intervals of 2 (SB) and 3 (MB) minutes, and accepted all solutions with SNR  $> 7$ . After the fringe fitting, the residual phase variations were found to be within  $3^\circ$  on the ground baselines, and  $< 10^\circ$  on the space baselines. We then averaged over all frequency channels, and calibrated the phases with a point source model (to enable time averaging). Finally, the data were exported into DIFMAP and further time-averaged into 60-second bins. The amplitude and phase errors were calculated from the scatter in the unaveraged data. Figure 2 gives an example of typical HALCA baseline visibility data. The estimated RMS noise on the

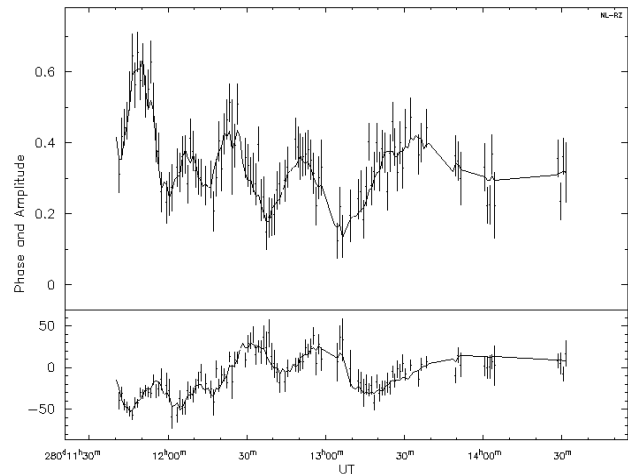


**Fig. 2.** Visibility amplitudes (top panel) and phases (bottom panel) on the baseline between HALCA and VLBA:North Liberty, after amplitude calibration, fringe fitting, and phase self-calibration. The lines drawn through the data represent the final CLEAN model of 0836+710.

HALCA baselines is about 4.5 times higher than on the ground baselines.

### 2.2. Imaging

To investigate the impact of the VSOP mission, we have imaged both the entire dataset (VSOP dataset hereafter) and only the ground baseline data (VLBA dataset), and compared the properties of these images. Both images have been produced after several cycles of hybrid mapping and self-calibration.

We use natural weighting for gridding the ground array data, enhancing the sensitivity to extended emission at the price of slightly decreased image resolution. The gridding weights are also scaled by amplitude errors raised to the power of  $-1$ . Both phase and amplitude self-calibration have been used, with amplitudes being allowed to vary only after the total model flux has approached the zero spacing flux to within 3%. The image obtained using this procedure is shown in the left panel of Figure 3.

To image the VSOP dataset, we use uniform weighting which provides a better angular resolution at the expense of lowering slightly the sensitivity to extended structures. Because the estimated noise on HALCA baselines is much higher than on the ground baselines, scaling the gridding weights by the amplitude errors weights down significantly all of the long  $uv$ -spacings. To avoid this, we switch off the amplitude scaling of gridding weights. As a safeguard measure, we apply only phase self-calibration to the VSOP dataset. After a good fit to the data is achieved, we adjust the antenna gains, correcting for small constant offsets between the model and the visibility amplitudes. An example of the obtained fit to the data can be found in

<sup>4</sup> The NRAO Astronomical Image Processing System

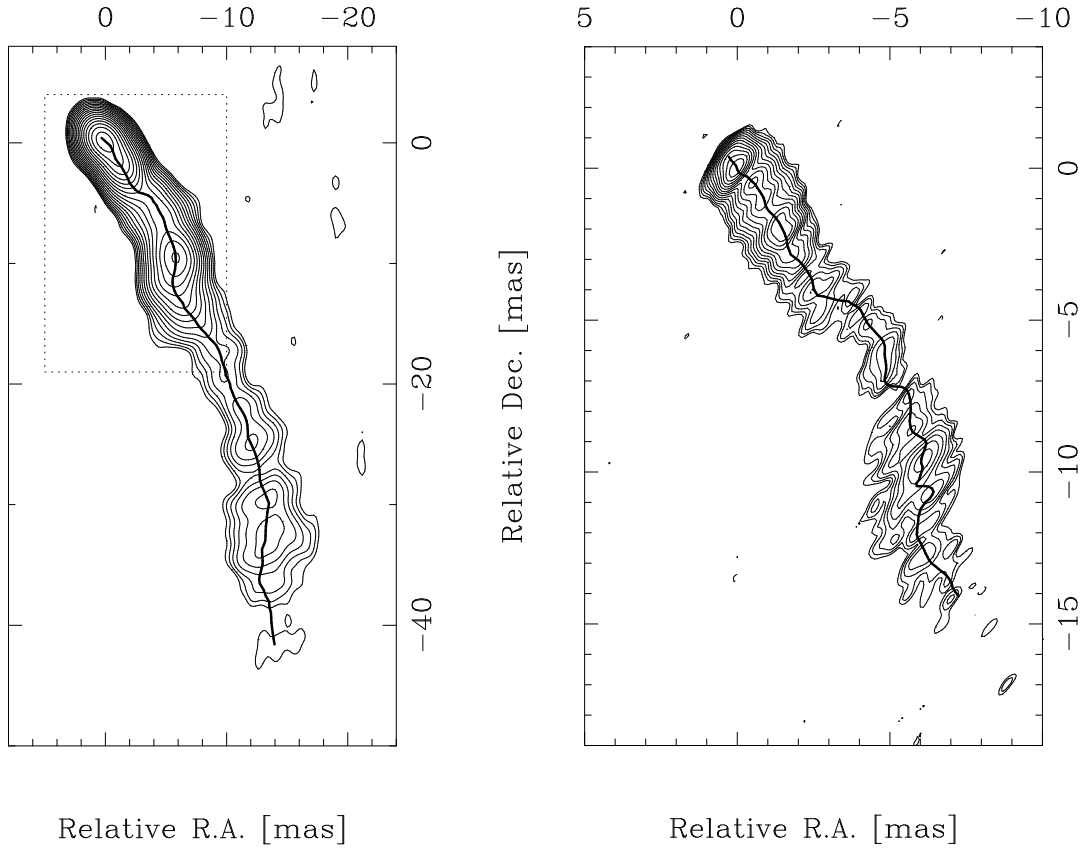


**Fig. 3.** Ground array (left) and VSOP (right) images of 0836+710, with the jet ridge line marked. In the ground array image, the dotted line rectangle shows the area covered by the VSOP image. The image parameters are as follows. The ground array image: restoring beam is  $2.15 \times 1.75$  mas at P.A. =  $30.8^\circ$ ; contour levels are drawn at  $-0.7, 0.7 \times 1.5^n$  mJy/beam ( $n = 0, \dots, 17$ ); the peak flux density is 918 mJy/beam. The VSOP image: restoring beam is  $0.93 \times 0.31$  mas at P.A. =  $-36.3^\circ$ ; contour levels are drawn at  $-1.5, 1.5 \times 1.5^n$  mJy/beam ( $n = 0, \dots, 13$ ); the peak flux density is 432 mJy/beam.

Figure 2. The final high-resolution image is shown in the right panel of Figure 3.

To test the reliability of the satellite data, we make an additional image using only the space baselines (HALCA image). The resulting image shown in Figure 4 is produced with only phase self-calibration applied. The structures seen in Figure 4 are consistent with the structures found in both VSOP and VLBA images in Figure 3. This reassures the good quality of the data received from the orbiting antenna.

Table 1 compares the properties of all three images. Note the roughly 5 times smaller dynamic range of the VSOP image, which is caused by the poorer sampling and increased noise of the data on the space baselines. The sufficiently high dynamic range of the HALCA image (200:1) reflects once again the high quality of the satellite data.

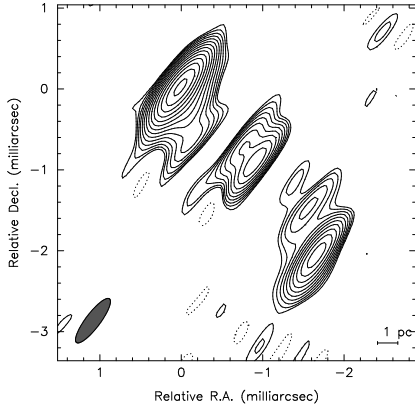
**Table 1.** Parameters of the images

Image (1)	$S_{\text{tot}}$ (2)	$S_{\text{max}}$ (3)	$S_{\text{min}}$ (4)	$\sigma_{\text{RMS}}$ (5)	$D_{\text{rms}}^{\text{peak}}$ (6)
VLBA	2.167	0.918	-0.001	0.2	4600:1
VSOP	2.156	0.432	-0.003	0.5	900:1
HALCA	0.731	0.325	-0.007	1.4	200:1

Column designation: 2 – total CLEAN flux [Jy]; 3 – peak flux density [Jy/beam]; 4 – lowest negative flux density [Jy/beam]; 5 – RMS noise [mJy/beam]; 6 – peak-to-RMS dynamic range.

### 3. Properties of the compact jet

In both VSOP and VLBA images, the jet is continuous, with several enhanced emission regions embedded in it. In Figure 4, curvature of the jet is noticeable even at  $\lesssim 1$  mas scales, and it is consistent with the images obtained at



**Fig. 4.** Image of 0836+710 obtained using only the baselines to HALCA. All structures seen in the image are consistent with those found in both the VSOP and VLBA images. This shows the reliability of the data recorded on the space baselines. The restoring beam is  $0.68 \times 0.18$  mas at P.A. =  $-36.9^\circ$ ; contour levels are drawn at  $-3.2, 3.2 \times 1.5^n$  mJy/beam ( $n = 0, \dots, 11$ ); the peak flux density is 325 mJy/beam.

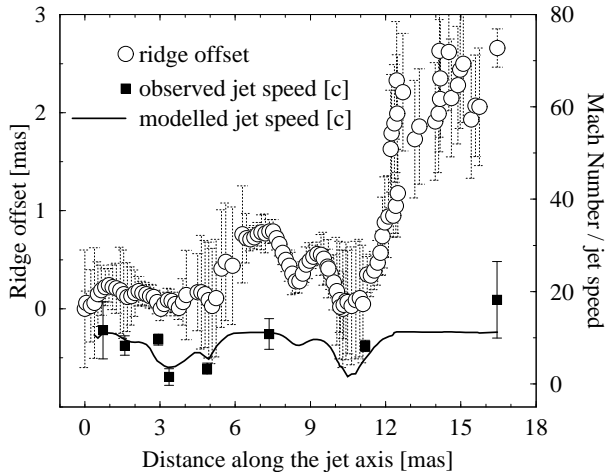


**Fig. 5.** Relation between the the ridge line and observed jet speeds in 0836+710. Circles are measured offsets of the jet ridge line from the jet axis at P.A. =  $-146^\circ$ ; squares denote speeds reported by Otterbein (1996) at different locations in the jet; solid line represents apparent speed variations derived from the measured ridge line offsets, for a jet with Mach number,  $M_j = 6$ , Lorentz factor,  $\gamma_j = 11$ , and opening half-angle,  $\phi_j = 1^\circ$ .

higher frequencies, most notably at 86 GHz (Otterbein *et al.* 1998). We consider now the observed curvature of the jet represented, in the maps in Figure 3, by the curved ridge line of the jet. We use the median P.A. =  $-146^\circ$  to approximate the direction of the jet axis, and measure the absolute values of corresponding offsets of the jet ridge line. The offsets are plotted in Figure 5 (opaque

circles). One can see that the offsets show a remarkable periodicity, possibly with several periods superimposed. The derived offsets also appear to be correlated with the apparent speeds measured along the jet (Otterbein 1996, black squares in Figure 5).

The apparent curvature of the jet may reflect the presence of plasma instabilities in the jet (e.g. MHD or Kelvin-Helmholtz instabilities). The amplitude of ridge line displacements from the jet axis can be used to estimate the jet Mach number,  $M_j$ , using the analytical approximation obtained by Hardee (1984) for the amplitude,  $\mathcal{G}(r)$ , of the fastest spatially growing mode of Kelvin-Helmholtz instability:  $\mathcal{G}(r) = \mathcal{G}(r_0)(r/r_0)^\epsilon$ . Here  $r$  refers to the distance along the jet axis, “0” denotes the initial values, and  $\epsilon$  is determined by the jet Mach number and opening half-angle,  $\phi_j$ , so that  $\epsilon = 0.83/(M_j \sin \phi_j)$ .

To quantify the initial conditions of the jet plasma, we adopt the results from Otterbein *et al.* (1998) obtained by modelling spectral evolution in the core of the VLBI jet in 0836+710. The initial amplitude of instability can then be approximated by the size of the core, so that  $\mathcal{G}(r_0) = 0.8$  pc, at  $r_0 = 15$  pc corresponding to the estimated distance from the jet nozzle to the core. With the reported jet bulk Lorentz factor,  $\gamma_j = 11$ , viewing angle,  $\theta_j = 3.2^\circ$ , and opening half-angle  $\phi_j = 1^\circ$ , we obtain the Mach number  $M_j \approx 6$ , within the innermost 3 mas of the jet. It is similar to the value reported in Otterbein 1996, and we take this as an argument in favor of our choice of the direction of the jet axis. We expect the inner jet to be pressure confined, with external pressure  $P_{\text{ext}} \approx 25 P_{\text{jet}}$ . Farther down the jet, at distances  $> 10$  mas ( $> 700 h^{-1}$  pc), the derived values of  $M_j$  appear to increase up to  $\sim 30 - 50$ , if we assume that the jet viewing angle remains the same.

Perhaps a more attractive possibility is to preserve the Mach number along the jet, and instead use variations of the jet viewing angle for explaining the observed ridge line offsets. For the same set of  $M_j$ ,  $\gamma_j$ , and  $\phi_j$ , we determine the variations of the viewing angle required to reproduce the offsets. The derived  $\theta_j$  changes smoothly between  $3^\circ$  and  $65^\circ$ , with largest values occurring at  $\sim 3$  mas and  $\sim 10$  mas distances — which are incidentally the locations where the most pronounced lateral displacements are reported (Krichbaum *et al.* 1990, Otterbein 1996). The combination of the assumed  $\gamma_j$  and derived  $\theta_j$  allows us to predict the apparent speed,  $\beta_{\text{app}}$ , along the jet. The predicted  $\beta_{\text{app}}$  (plotted in Figure 5 with the solid line) is in a reasonable agreement with the measured jet speeds. At  $r > 13$  mas, the predicted  $\beta_{\text{app}}$  becomes flat, as it approaches the limit of  $(\gamma_j^2 - 1)^{1/2}$ . At distances  $r > 15$  mas, a moderate increase of  $\gamma_j$  up to  $\sim 15$ , could provide a better agreement with the measured speed. However, at these distances, the measurement uncertainties for both the speeds and ridge line offsets are too large to warrant arguing in favor of variable bulk speeds along the jet. We would like to emphasize that the achieved consistency between the model

and observed speeds is preserved, if the chosen direction of the jet axis are within a few degrees from the one we have used. In that case, only the derived jet Mach number would have differed from  $M_j = 6$  obtained above. Sparsity of the available speed measurements precludes better kinematic modelling and selecting the jet axis unambiguously. We expect that making such a selection would require determining the continuous velocity distribution along the jet, for which a suitable monitoring program should be designed, aimed at obtaining a sequence of high dynamic range and high fidelity VLBI images of the source.

#### 4. Conclusions

The reported observation of 0836+710 shows that the VSOP mission provides an excellent opportunity for high-resolution and high dynamic range imaging of VLBI-scale jets in extragalactic objects. The obtained VSOP image of 0836+710 allows to investigate the jet morphology and physical conditions on linear scales up to 1 kpc. We have studied the curved ridge line in the jet, and shown that, on the scales of  $\lesssim 700h^{-1}$  pc, it can be modelled by a pressure confined relativistic outflow with Lorentz factor  $\gamma_j \approx 11$ , Mach number  $M_j \approx 6$ , and opening half-angle  $\phi_j \approx 1^\circ$ . In this description, the two main factors responsible for the observed curvature of the jet ridge line are: 1) Kelvin-Helmholtz instabilities developing in the relativistic plasma and 2) variations of the angle,  $\theta_j$ , between the velocity vector of the outflow and the line of sight. We have shown that the derived variations of  $\theta_j$  can be used for predicting the jet kinematics, and are consistent with the observed variable apparent speeds along the jet.

#### Acknowledgements

We gratefully acknowledge the VSOP Project, which is led by the Japanese Institute of Space and Astronautical Science in cooperation with many organizations and radio telescopes around the world. We thank R. Porcas and J. Marcaide for constructive comments on the manuscript. The National Radio Astronomy Observatory is a facility of the National Science Foundation operated under cooperative agreement by Associated Universities, Inc.

#### References

- Brunner H., Lamer G., Staubert R., Worall D. M., 1994, *A&A* 287, 436.  
 Fichtel C. E. Bertsch D. L., Chiang J. et al., 1994, *ApJS*, 94, 551.  
 Hardee, P.E. 1984, *ApJ*, 287, 523.  
 Hirabayashi, H. 1996, *Springer Science (Quarterly)* 2, 11, 6.  
 Hummel C. A., Muxlow T. W. B., Krichbaum T. P. et al., 1992, *A&A*, 266, 93.  
 Krichbaum T.P., Hummel C.A., Quirrenbach A. et al., 1990, *A&A*, 230, 271.  
 von Linde J., Borgeest U., Schramm K.-J. et al., 1993, *A&A* 267, L23.

- Marscher A. P. & Bloom S. D. 1994, in: *Compact Extragalactic Radio Sources*, ed. J.A. Zensus and K.I. Kellermann (NRAO, Socorro), p. 179.  
 Otterbein K., 1996, PhD thesis, University Göttingen.  
 Otterbein K., Krichbaum, T. P., Kraus, A., et al. 1998, 334, 489.  
 Shepherd M. C., Pearson, T. J., & Taylor, G. B. 1994, *BAAS* 26, 987.  
 Zensus, J. A., Diamond, P. J., & Napier, P. J. (eds.) 1995, "Very Long Baseline Interferometry and the VLBA", ASP Conference Series, Vol. 82.